Three-dimensional Simulations for Void Fraction Distribution in a Two-component Two-phase Flow System

Sanjeev Kumar, Arun K. Saha and Prabhat Munshi
Indian Institute of Technology Kanpur, Kanpur 208016, India
(sanjeevk@iitk.ac.in, aksaha@iitk.ac.in , pmunshi@iitk.ac.in)

Abstract

This work focuses on the three-dimensional simulation of two phase flows. Experimental data (obtained previously for a mercury-nitrogen flow loop) was processed by computerized tomography and the results were compared with Fluent6.1®. It was found that void fraction predictions by two approaches were different for higher flow rates. This work included the new analysis and compared with the old analysis results and experimental results for similar experimental conditions. New analysis has been done by using latest software platform ANSYS Fluent14.0® with different model (Eulerian) options available in the code. We observe that the predictions by Eulerian model are much closer to the experimental results as compared with the earlier work using mixture model.

1. Introduction

Multi-phase processes are commonly used in many industrial fields, e.g. nuclear reactors and chemical reactors (bubble column reactor) [1, 2]. The distribution of phases and how they interact with each other is still a field of research. Bubble columns are commonly used among the equipments for such type of processes. They are inexpensive reactors and easy to operate. One such set-up was developed at Bhabha Atomic Research Centre (Mumbai, India) and some results have already been reported by Saksena et al. [3]. It consists liquid metal magneto hydrodynamic (LMMHD) loop that incorporated two-phase flow of mercury and nitrogen in the riser leg of the flow loop. Nitrogen gas was injected at the bottom to circulate mercury through the entire loop. Mercury (liquid metal) passes through the strong poles of magnet (attached to the downcomer of the setup) and produces the power [1, 2, 3]. Forced convection is the dominant phenomena as nitrogen is expected to carry the flow of mercury upwards against the gravity. Void fraction distribution is necessary to design such system [3]. Experiments were performed to measure this parameter, non-invasively (gamma-ray tomography) in the riser leg of the loop. This distribution was at 1.1 m height of the riser leg and it was also determined numerically by commercially available CFD code Fluent6.1®. Mixture model was used to simulate the riser leg of the experimental setup. It was observed that simulation results deviated substantially from the experimental results for high flow rate of nitrogen. The present work is an attempt to understand this mismatch by performing the same study work by the latest version of this code (ANSYS Fluent14.0®). Multiphase Eulerian model is used here in place of mixture model. Flow pattern is governed by the inter-phase interaction, external boundary conditions and material properties. It also depends upon the flow regimes, i.e. bubbly, churn, slug and annular. The flow regimes considered in this work vary from churn-turbulent to bubbly flow [3, 4]. The standard k-ε turbulence model is used with enhanced wall treatment and per phase basis [5] has been used.

These simulation results now are much closer to the experimental results as compared to the earlier work [3].

2. Experimental and Computational Details

We have chosen to base our investigations on published work (Saksena et al. [3]) to compare our simulations with experimental and simulated data already reported. Schematic of that experimental set-up is shown in Figure 1(a) and computational domain in Figure 1(b). Simulations have been done for the riser leg which has an internal diameter 78 mm and height 1.9 m. Three different flow rates of nitrogen 20, 40 and 60 liter/min (2.39×10^{-3}, 4.48×10^{-3} and 6.94×10^{-3} kg/s) were considered. The corresponding mercury flow rates were 20.5, 25.5 and 27.5 kg/s. Operating pressure was 5.69 bars and the temperature of the mercury was 165^{0}C. We refer to earlier published works [3, 6] for more details about experimental setup and data collection geometry. Uncertainty analysis of the experimental work has already been presented by Jayakumar et al. [7].

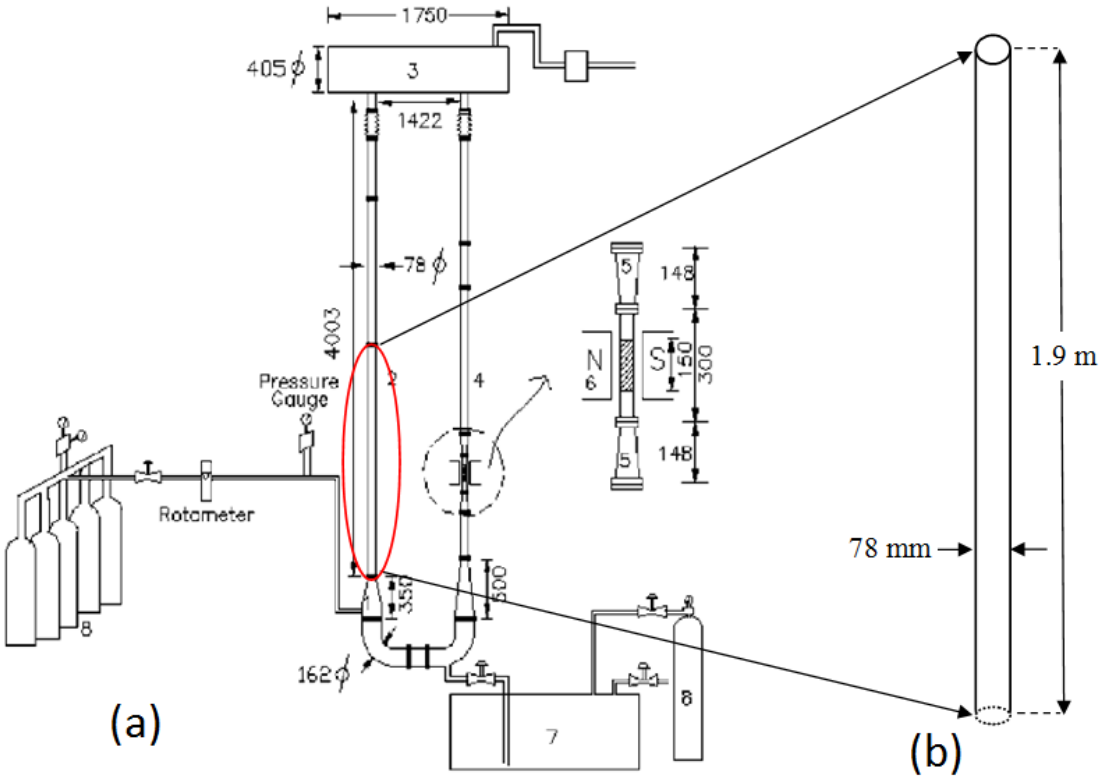

Figure 1 (a) Schematic of LMMHD power converter loop facility (1 = mixer, 2 = riser, 3 = separator, 4 = downcomer, 5 = transitional pieces, 6 = MHD generator and magnet, 7 = dump tank, 8 = nitrogen cylinders) from Saksena et al. [3], (b) Solution domain.

Numerical simulations has been carried out in a full 3D, unsteady Euler-Euler framework by means of the commercial software ANSYS Fluent14.0®. Mesh has been created with the help of software Gambit 2.4. Parallel processing on Intel(R) core(TM) i7-2600K CPU @ 3.40 GHz has been used to perform the simulations. Usually 6-8 processors have been used.

Lapin and Lubbert [8] proposed Euler-Euler and Euler-Lagrange models to predict the multiphase flow structure in bubble columns. Euler-Lagrange model is suitable for low discrete phase volume fraction (less than 10%) cases and Euler-Euler model is suitable for high discrete phase volume fraction cases [5, 9]. Euler-Euler model has been used in the present work due to high discrete phase volume fraction. A single pressure is shared by all the phases in this model. Momentum and continuity equations are solved for each phase.

Volume fractions represent the space occupied by each phase and the laws of conservation of mass and momentum are satisfied by each phase individually. The volume of phase q, V_q is defined by

$$V_q = \int_V \alpha_q dV \tag{1}$$

where,

$$\sum_{q=1}^{n} \alpha_q = 1$$

where α_q is the volume fraction of q^{th} phase and n is total number of phases.

The continuity equation (conservation of mass) for phase q is given by

$$\frac{\partial}{\partial t}\left(\alpha_q \rho_q\right) + \nabla \cdot \left(\alpha_q \rho_q \vec{v}_q\right) = \sum_{p=1}^{n}\left(\dot{m}_{pq} - \dot{m}_{qp}\right) + S_q \tag{2}$$

where $\vec{v}_q$ is the velocity of q^{th} phase, $\dot{m}_{pq}$ is the mass transfer from p^{th} to q^{th} phase and S_q is the source term. Both the terms on the right hand side of above equation are zero in this work, because there is no inter-phase mass transfer and no mass generation.

Momentum conservation equation for q^{th} phase is given by

$$\begin{aligned}\frac{\partial}{\partial t}\left(\alpha_q \rho_q \vec{v}_q\right) + \nabla \cdot \left(\alpha_q \rho_q \vec{v}_q \vec{v}_q\right) = -\alpha_q \nabla p + \nabla \cdot \overline{\overline{\tau}}_q + \alpha_q \rho_q \vec{g} + \sum_{p=1}^{n}\left(\vec{R}_{pq} + \dot{m}_{pq}\vec{v}_{Pq} - \dot{m}_{qp}\vec{v}_{qp}\right) \\ + \left(\vec{F}_q + \vec{F}_{lift,q} + \vec{F}_{vm,q}\right)\end{aligned} \tag{3}$$

where $\overline{\overline{\tau}}_q$ is q^{th} phase stress-strain tensor and is given by

$$\overline{\overline{\tau}}_q = \alpha_q \mu_q \left(\nabla \vec{v}_q + \nabla \vec{v}_q^T \right) + \alpha_q \left(\lambda_q - \frac{2}{3} \mu_q \right) \nabla \cdot \vec{v}_q \overline{\overline{I}}$$

where μ_q and λ_q are the shear and bulk viscosity of the q[th] phase. $\vec{F}_q$ is an external body force, $\vec{F}_{lift,q}$ is lift force, $\vec{F}_{vm,q}$ is virtual mass force acting on the q[th] phase. $\vec{R}_{pq}$ is interaction force between phases, p is pressure shared by all the phases and $\vec{v}_{Pq}$ is the interphase velocity. $\overline{\overline{I}}$ is the unit tensor.

Lift force is negligible compared to the drag force in most of the cases. Virtual mass force is not included in the present work due to the lack of sufficient experimental information. This force will be included in the future work.

Following formula is implemented through User Defined Function (UDF) in ANSYS Fluent14.0®. Bubble diameter of nitrogen at pressure P is

$$d = d_{ref} \left(\frac{P_{ref}}{P} \right)^{1/3} \tag{4}$$

where d_{ref} is the bubble diameter at the reference pressure $P_{ref.}$

k-ε turbulence model has been used in the present work. ANSYS Fluent14.0® has three options for k-ε turbulence model: mixture turbulence model, dispersed turbulence model and turbulence model for each phase. k-ε mixture turbulence model is applicable when the density ratio between the phases is close to 1 [5]. This model is not applicable in the present work because the density ratio of mercury and nitrogen is far away from 1. k-ε dispersed turbulence model is an appropriate model when the concentrations of the secondary phases are dilute (less than 10%). This model is also not applicable in the present work because concentration of the secondary phase is greater than 10%. k-ε turbulence model for each phase is used in the present work because this model is an appropriate model when the turbulence transfer among the phases plays a dominant role.

Computational model described above was solved using commercial flow software ANSYS Fluent14.0®. This works on the finite volume method. The region above the mixer, up to the half of the length (1.9 m) of the upcomer, was considered to be the computational domain. The internal diameter of the upcomer was taken to be 78 mm. Three-dimensional geometry of the upcomer was created using grid generation tool Gambit2.4. The domain is meshed with unstructured grid, and the volume elements are of hexahedral shape to minimize skewness [10], by cooper algorithm. A wall type of boundary condition has been used for the pipe wall. Mass flow inlet type of boundary condition has been used to specify the flow rate at the inlet. Pressure outlet type of boundary condition has been used to specify the flow at the outlet. Different sets of grids were generated (number of computational cells varying from 704 to 84584). Typical grid used in the present work is shown in Figure 2.

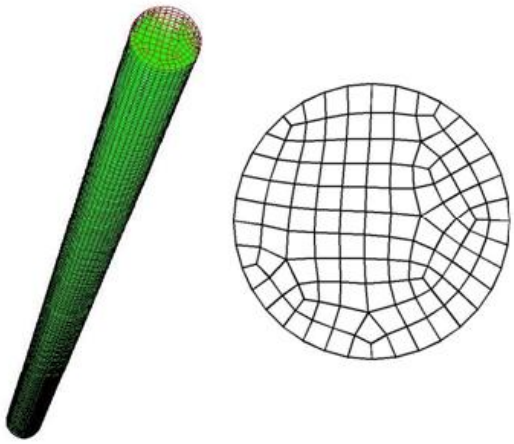

Figure 2 Computational mesh.

The domain has been initialized based on the values at the inlet. The time step has been taken to be 0.001 s to satisfy the CFL condition. Flow is averaged to a total time of 76 s. Pressure-velocity coupling has been done by the scheme coupled. Quadratic Upwind Interpolation for Convective Kinetics (QUICK) is used to spatially discretize the volume fraction. 2nd order upwind scheme is used to spatially discretize the other physical quantities (momentum, k, ε). Transient formulation has also been done by 2nd order upwind scheme and symmetric drag law [5] is used.

3. Grid Independence Study

A test case has been performed to make the grid independent solution. This test case has been done for a particular flow rate with different grids (number of computational cells varying from 704 to 84584). Average void fraction of nitrogen at 1.1 m height from the inlet has been chosen as the parameter to check the grid independence. Variation of average void fraction of nitrogen at a height of 1.1 m from inlet with grid size has been shown in Table 1. This variation has also been plotted in Figure 3.

S. No.	Grid Size (m)	No. of Volume Elements	Average Void Fraction at 1.1 m	% change in results on refinement of grid
1	0.03	704	0.1452	
2	0.02	2162	0.1411	2.82
3	0.01	12928	0.1378	2.35
4	0.009	18312	0.1375	0.25
5	0.008	22072	0.1368	0.50
6	0.007	33201	0.1378	0.76
7	0.006	54442	0.1379	0.04
8	0.005	84584	0.1378	0.05

Table 1 Grid independence test

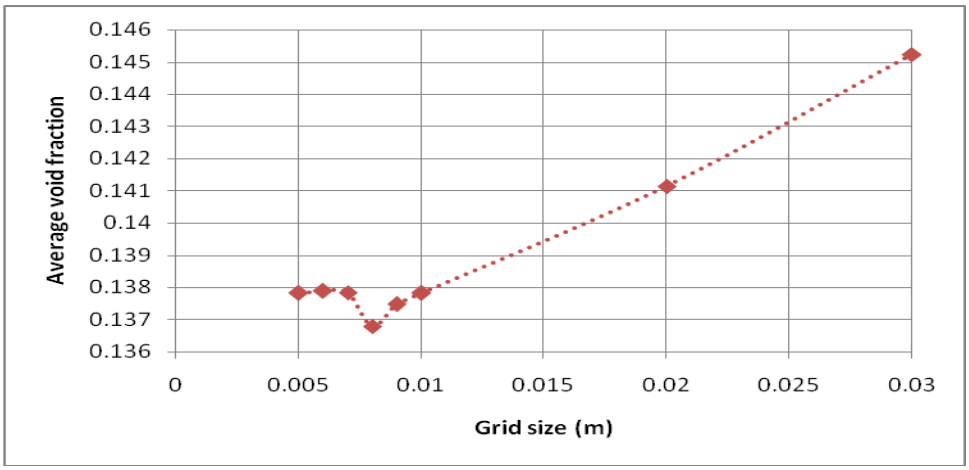

Figure 3 Average void fraction of nitrogen at 1.1 m vs. Grid size.

It is clear that for the grid refining from 0.03 m to 0.02 m, the percentage change in solution is 2.82 %. Percentage change in solution decreases with refining the grid again. It is only 0.04% when we refined the grid from 0.007 m to 0.006 m. It is also clear from Figure 3 that there is no substantial change in solution refining more than 0.007 m. Thus a grid size of 0.007 m with 33201 volume elements has been chosen for the problem under study.

4. Results and Discussion

Void fraction distribution throughout the column has been analyzed. Void fraction distribution of the nitrogen at a cross-sectional plane of the bubble column at a height of 1.1m from the inlet has been presented. Three different flow rates of nitrogen (20 LPM, 40 LPM and 60 LPM) have been considered.

Contour plots of nitrogen void fraction distribution for all the three cases of nitrogen flow rates of 20 LPM, 40 LPM and 60 LPM are shown in the Figure 4(A), Figure 4(B) and Figure 4(C) respectively. Red colour shows the maximum value and blue colour shows minimum value of the void fraction of Nitrogen.

Void fraction of nitrogen is higher in the annular region for low flow rates of nitrogen (Figure 4). It is also clear that as the flow rate increases (void fraction of nitrogen increases), the void fraction of nitrogen starts to disperse throughout the column. This fact is physically obvious.

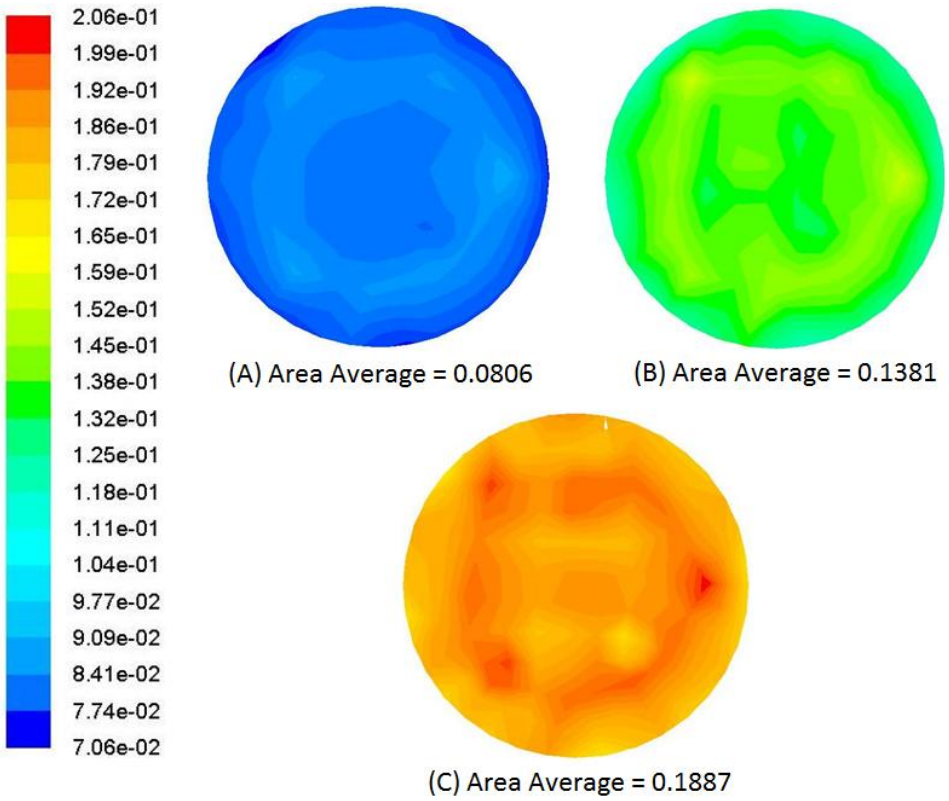

Figure 4 Contour plots of void fraction of nitrogen at a height of 1.1 m for flow rates of nitrogen (A) 20 LPM,(B) 40 LPM, (C) 60 LPM

Latest simulated (Eulerian model) results have been compared with the simulated (mixture model) and experimental results already reported by Saksena et al. [3] in the Table 2.

Flow rate (LPM)	**Predicted Area Average (Ref. [3])**	**Predicted Area Average (Eulerian model)**	**Experimental Area Average (Ref. [3])**	**% Mismatch (Ref. [3])**	**% Mismatch (Eulerian model)**
20	0.098	0.0806	0.09	8.16	10.44
40	0.18	0.1381	0.13	27.7	6.23
60	0.29	0.1887	0.19	34.48	0.68

Table 2 Comparison of the results

Predicted void fraction of nitrogen for the flow rate of 20 LPM is less than its corresponding experimental value (0.09). In this particular case (20 LPM), void fraction of secondary phase (nitrogen) is less than 10%. Euler-Lagrange (computationally expansive) model is more suitable than the Euler-Euler model for the case of secondary phase void fraction less 10% [11]. Euler-

Euler model is used for all the cases in present work due to the limitation of the computational effort. Authors believe that Euler-Lagrange model will give better results than Euler-Euler model for this case (20 LPM). Predicted area average of nitrogen for the cases of 40 LPM and 60 LPM is very close to its experimental value.

It is clear that the latest simulated (Eulerian model) results are very close to the corresponding experimental results. The percentage mismatch of the results is less than 11% for all cases. This model is suitable for low as well as high flow rates of nitrogen. This model rectifies the shortcomings (not applicability for high flow rates) of old model.

Simulated results of radial distribution of velocity magnitude of mercury (Hg) and nitrogen (N_2) at different flow rates at a height of 1.1 m from the inlet are shown in the Figure 5. Comparison of these results with the experimental results is not presented here due to the unavailability of the corresponding Experimental results. Velocity magnitude is maximum at the centre and it is zero near the wall. Magnitude of the velocity increases with the increase of the flow rates. Velocity of nitrogen is always greater than the velocity of mercury.

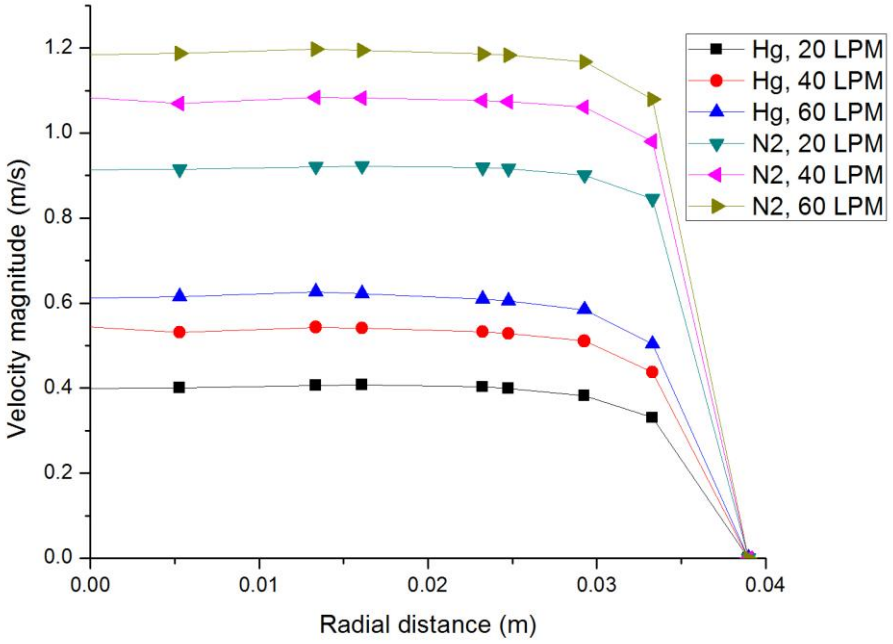

Figure 5 Radial distribution of velocity magnitudes of mercury (Hg) and nitrogen (N2) at a height of 1.1 m from the inlet for different flow rates of nitrogen

5. Conclusions

This work included the new analysis and compared with the old analysis results and experimental results for similar experimental conditions. New analysis has been done by using latest software platform ANSYS Fluent14.0® with different model (Eulerian) options available in the code. It has been observed that new analysis results are much closer to the experimental results as compared with the earlier work using mixture model. This update is now applicable for low as well as high flow rates, as old analysis was not acceptable for high flow rates. Main conclusions are as follows:

1) Quantitative results of new analysis are very much similar to the experimental results for all flow rates. There is a small mismatch between the results for the case of 20 LPM (void fraction of secondary phase less than 10%). This may be reduced by using Euler-Lagrange (computationally expensive) model in place of using Euler-Euler model.

2) Void fraction distribution of nitrogen is high in the annular region for low flow rates (low void fraction) of nitrogen.

3) Void fraction of nitrogen increases in the near wall as well as central region with the increase of flow rate of nitrogen. This fact is physically acceptable, because as the flow rate increases, void fraction of nitrogen increases and hence it dispersed throughout the column cross-section.

4) New analysis (using Eulerian model) is applicable for low as well as high flow rates of nitrogen, as the old analysis (with mixture model) was not acceptable for high flow rates.

5) Velocity is maximum at the centre and zero at the wall. Velocity of mercury and nitrogen increases with the flow rates. Velocity magnitude of nitrogen is approximate double of the corresponding velocity magnitude of nitrogen.

6. Nomenclature

d_{ref}	bubble diameter at reference pressure, m	$\vec{F}_q$	external body force, N/m^2
$\vec{F}_{lift,q}$	lift force on qth phase, N/m^2	$\vec{F}_{vm,q}$	virtual mass force on qth phase, N/m^2
$\vec{g}$	gravitational acceleration, m/sec^2	$\overline{\overline{I}}$	unit tensor
μ_q	shear viscosity of qth phase, kg/m.sec	λ_q	bulk viscosity of qth phase, kg/m.sec
$\dot{m}_{pq}$	mass transfer from pth to qth phase, kg/sec	p	pressure sheared by all phases, N/m^2
p_{ref}	reference pressure, N/m^2	ρ_q	density of qth phase, kg/m^3
$\vec{R}_{pq}$	interaction force between phases, N/m^2	S_q	source term of qth phase, kg/sec
$\overline{\overline{\tau}}_q$	qth phase stress-strain tensor	$\vec{v}_q$	velocity of qth phase, m/sec
$\vec{v}_{Pq}$	interphase velocity, m/sec	V_q	volume of qth phase, m^3

α_q void fraction of q^{th} phase, dimensionless

7. References

[1] G. Fabris and R. G. Hantman, "Fluid Dynamic Aspects of Liquid-Metal Gas Two-Phase Magnetohydrodynamic Power Generators", *Proceedings of the 1976 Heat Transfer and Fluid Mechanics Institute*, pp. 92-113

[2] Gutierrez-Miravete, Ernesto and Xiaole, Xie, "A Study of Fluid Flow and Heat Transfer in a Liquid Metal in a Backward-Facing Setup under Combined Electric and Magnetic Fields", *Proceedings of the 2011 COMSOL Conference in Boston*.

[3] R. Saksena, P. Satyamurthy, P. Munshi, "A comparison of experimental results and fluent simulations for void-fraction distribution in a two-phase system", *Nuclear Technology*, vol. 163, 2008, pp. 426–434.

[4] Cédric Laborde-Boutet, Faiçal Larachi, Nicolas Dromard, Olivier Delsart, Daniel Schweich, "CFD simulation of bubble column flows: Investigations on turbulence models in RANS approach", *Chemical Engineering Science*, vol. 64, 2009, pp. 4399–4313.

[5] ANSYS Fluent14.0 Theory guide, November 2011, ANSYS Inc., Southpointe, 275 Technology Drive, Canonsburg, PA 15317

[6] T.K. Thiyagarajan, P. Satyamurthy, N.S. Dixit, N. Venkatramani, "Void Fraction Profile Measurements in Two-Phase Mercury-Nitrogen Flows Using Gamma-Ray Attenuation Method", *Experimental Thermal and Fluid Science*, vol. 10, 1995, pp. 347–354.

[7] P. Jayakumar, P.Munshi, "A comprehensive study of measurement uncertainty in tomographic reconstruction of void-profiles in a mercury-nitrogen flow", *Experiments in Fluids*, vol. 26, 1999, pp. 535–541.

[8] Lapin, A., & Lubbert, A., "Numerical simulations of the dynamics of two-phase gas–liquid flows in bubble columns", *Chemical Engineering Science*, vol. 49, 1994, pp. 3661–3674.

[9] M.A. Behbahani, M. Edrisi, F. Rashidi, E. Amani, "Tuning a multi-fluid model for gas lift simulations in wells", *Chemical engineering research and design*, vol. 90, 2012, pp. 471–486.

[10] Akio Tomiyama, Hidesada Tamai, Iztok Zun, Shigeo Hosokawa, "Transverse migration of single bubbles in simple shear flows", *Chemical Engineering Science*, vol. 57, 2002, pp. 1849–1858.

[11] Mohan R. Rampure, Amol A. Kulkarni, and Vivek V. Ranade, "Hydrodynamics of Bubble Column Reactors at High Gas Velocity: Experiments and Computational Fluid Dynamics (CFD) Simulations", *Ind. Eng. Chem. Res.*, vol. 46, 2007, pp. 8431–8447.